Control Engineering Practice

Self-sensing active control of emulated tangential tool vibration hardware-in-the-loop

--Manuscript Draft--

Manuscript Number:	CONENGPRAC-D-20-00501R1
Article Type:	Regular article
Keywords:	Active vibration control, emulated tool vibration, self-sensing actuator, adaptive feedback active noise control, linearization.
Corresponding Author:	Burkhard Heinrich Freyer, Ph.D. University of Pretoria Pretoria, SOUTH AFRICA
First Author:	Burkhard Heinrich Freyer, Ph.D.
Order of Authors:	Burkhard Heinrich Freyer, Ph.D.
	Nicolaas J Theron, Ph.D.
	Phillippus S Heyns, Ph.D.
	Lutz A Pickelmann, Dr. rer. nat.
Abstract:	This study tests the dual functionality of a piezoelectric transducer for active control of emulated tool vibration. The concept of a self-sensing actuator is here applied jointly with adaptive feedback active vibration control as hardware-in-the-loop. It controls pre-recorded tangential tool vibrations at the tool holder's first bending mode. This work shows that the selected building blocks of the complete control loop are key to the design. It opens perspectives for a single transducer design and a simultaneous tool condition monitoring function. 10 dB attenuation of tool vibrations, bending-mode-focussed control command and feedback signal-to-noise-ratio of 20 demonstrate the system's functionality.

Title: **Self-sensing active control of emulated tangential tool vibration hardware-in-the-loop**

Running headline: Self-sensing active tool vibration control

Burkhard H. Freyer[a *] Nico J. Theron[b] P. Stephan Heyns[b] Lutz A. Pickelmann[c]

[a] *Department of Mechanical and Aeronautical Engineering, University of Pretoria, 0002 Pretoria, South Africa*

[b] *Centre for Asset Integrity Management, Department of Mechanical and Aeronautical Engineering, University of Pretoria, 0002 Pretoria, South Africa*

[c] *Piezomechanik GmbH, Berg-am-Laim-Straße 64, D-81673 Munich*

[*]Corresponding author:

Tel. (via N.J. Theron): +27-(0)12-4203309

Fax. . (via N.J. Theron): +27-(0)12-3625087

Email: burkhard.freyer@gmail.com

Declaration of Interests

The authors declare that there is no potential conflict of interests.

Acknowledgements

Research:

Funding by The National Research Foundation of South Africa [grant number 2053282], the University of Pretoria and assistance by World Test Systems and Texas Instruments in South Africa by respectively borrowing and donating equipment is gratefully acknowledged. The authors appreciate the access to Matlab software permitted by the Senior PC Support of the Namibia University for Science and Technology.

Personal:

BHF acknowledges the maintenance support of his father Eckhart Freyer

Highlights of Article:

Title: **Self-sensing active control of emulated tangential tool vibration hardware-in-the-loop**

- Functionality of self-sensing actuator in tool vibration control established.
- Proposed tool vibration control compares favourably with equivalent technology.
- Key design considerations with actuator concept demonstrated or addressed.
- A single transducer can now be used for feedback tool vibration control.
- Truly collocated sensor and actuator improve system stability properties.

Abstract

This study tests the dual functionality of a piezoelectric transducer for active control of emulated tool vibration. The concept of a self-sensing actuator is here applied jointly with adaptive feedback active vibration control as hardware-in-the-loop[1]. It controls pre-recorded tangential tool vibrations at the tool holder's first bending mode. This work shows that the selected building blocks of the complete control loop are key to the design. It opens perspectives for a single transducer design and a simultaneous tool condition monitoring function. 10 dB attenuation of tool vibrations, bending-mode-focussed control command and feedback signal-to-noise-ratio of 20 demonstrate the system's functionality.

.

Keywords

Active vibration control, emulated tool vibration, self-sensing actuator, adaptive feedback active noise control, linearization.

1. Introduction

Several accompanying advantages for the turning process are driving research on tool vibration control. Authors in [1] show that control of tool vibration results in increase of stability regions.

---

[1] HIL: hardware-in-the-loop
PIL: processor-in-the-loop
LMS: least-mean-square
AFANC: active-feedback-anti-noise-control
AVC: active vibration control
DSP: digital signal processor
SNR: signal-to-noise-ratio
ANN: Artificial neural network
TCM: tool condition monitoring
RTDX: real-time data exchange
codec: coder-decoder
SSA: self-sensing actuator
SC: sensing circuit
FIR: finite impulse response
FRF: frequency response function
RBF: Radial basis function

This stabilization means that regions with certain cutting parameter selections formerly related to unstable operating conditions can now be used for cutting, thus improving productivity. In addition to that do control systems, that are adaptive, allow for operating across different process parameter settings, resulting in increased machining flexibility. Studies in literature show, that the control of vibrations will reduce work piece surface roughness and tool wear. ([2], [3], [4], [5]).

Introduction of piezoelectric actuators came to advance active control of tool vibration ([6], [7]). However besides their function as actuators they have a sensing capability. From a literature perspective work of [8] is one of the most recent pieces of research utilizing this principle. In the transducer's sensor function an impedance bridge sensing circuit with a passively matched reference impedance aids to extract the sensed signal, which can be deformation of the structure it is attached to.

Pieces of literature present the task of matching the reference to the self-sensing actuator's (SSA) impedance as balancing task. In a bridge circuit it is actively balanced during operation using an adaptive LMS algorithm ([9],[10], [11]).

Literature brought up this self-sensing principle before, with focus on the principle itself. Its application, as related to a turning process and associated system design aspects, is the novelty this paper deals with ([12],[13]). The particular application of the SSA in feedback control of tool vibrations furthermore lends itself for use in simultaneous tool condition monitoring (TCM) by exploiting tool wear sensitive features in the control loop feedback signal ([14],[15]). The SSA would thus combine feedback control and simultaneous TCM using a single transducer.

The proposed system for the control of emulated tool-vibrations here comprises two essential building blocks. One is the sensing circuit as the hardware building block basically adopted from [13]. The other is a DSP-embedded adaptive feedback active noise control algorithm (AFANC), as proposed by [16], and is the software building block. The main goal of this work is to prove system functionality by demonstrating that above mentioned building blocks are functional as a complete system. It includes consideration given to sensing circuit balancing, actuator linearization, model identification. The actuator position in the tool holder furthermore poses the conflicting requirements of providing sensitivity in its sensor function and direct action in its actuator function. These requirements become addressed. This initial stage therefore uniquely engages established principles and methods in a way to represent a control system for the purpose of single transducer active tool vibration control which is here a new application. This study's solution to the problem of emulated tangential tool vibrations will show how the point of functionality was reached.

Towards reaching above mentioned objective, the tool vibrations, being the main problem of machining operations, are here targeted on the effect and not on the cause level. These effects are the load disturbance on the tool holder and are here controlled directly.

Control system simplicity is the reason for choosing this approach for now. It saves modelling effort costs of the cause of these vibrations, such as their regenerative nature and tool-work-piece dynamics.

The paper consists of five main sections. The second section is material and methods and it gives detail of the experimental set-up and test signals, further detail of the hardware building block, viz. the sensing circuit, its equations and the balancing and test procedure. The third section is theory and calculations and has the model identification performed, inclusive of linearization measures for the SSA. It also gives account of the control system. This and the preceding one, discussing model identification, consider the basis for the information coded for the DSP. They relate to the software building block. The fourth section are the results and discussion with limitations. This includes a comparison with competing technologies and finally the fifth section is the conclusion.

2. Material and Methods

2.1 Set-up and test signals

2.1.1 The set-up

A representative tool holder, clamped in a representative tool post, makes up the test structure shown in Figures 1 and 2. Part of this is the SSA stack, which was under inherent pre-compression as well as pre-compression from contact with the tool holder substitute. The line of action of the SSA stack actuator is perpendicular to the tool holder. Its force on the tool holder is directly opposite to the representative tangential cutting force exerted by the shaker stinger onto the tool holder. A spherical actuator tip was mating with a flat surface on the tool holder substitute at node 2 to avoid damaging cant of the piezo ceramic stack. Thus positive form locking between the SSA and the representative tool holder was unidirectional and existed only for the pushing action of the SSA. This means that the actuator can only push against the tool holder when it is expanding, but cannot pull the tool holder when it is contracting. The SSA's position is at an offset from the shaker force application point, node 1, to increase the shaker force lever on the SSA. The increased leverage causes the SSA to be more sensitive to the tool tip deflection, i.e., node 1 displacement.

The test vibration signals used in this study were previously recorded as tangential cutting force signals, from a real turning process. In this HIL experiment theses signals drive a shaker to emulate the tangential cutting force component resulting in tangential tool vibration. The force transducer in the shaker's connection to the tool holder via a stinger provides a signal of the force applied.

The main part of the solution to the vibration problem lies in two building blocks, viz. the DSP with embedded feedback control algorithm and the sensing circuit (SC) with integrated SSA. The AFANC control algorithm embedded on the DSP determines a control command, V_{i1}, from the strain proportional signal, V_{sens}. The control command signal, V_{i1}, drives the voltage amplifier, which in turn with voltage, V_{in}, drives the SSA, which is the active leg of the SC bridge. The purpose of the band-pass filter in SC, with V_{sens} as output, is to make the first bending mode in the forward path transfer function, discussed in section 3.3.1, stand out clearly.

The experimental procedure follows and Table 1 lists the equipment for the experiment.

2.1.2 Test signals

The test signals for this work originate from cutting force measurements with a strain gauge instrumented tool holder in a turning process under the following conditions ([15]):

1. Lathe: Colchester Student (manually operated).
2. Cutting parameters: cutting speed, feed rate and depth of cut respectively having been 1.44 to 1.61 m/s, 0.3 mm/rev and 1 mm.
3. Method: measurements were conducted and statically calibrated according to the method described in work by [15].

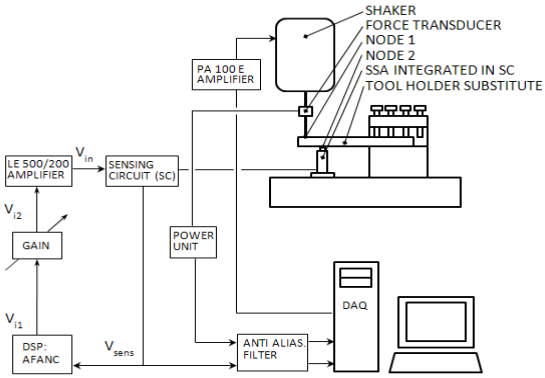

Fig1 Experimental set-up for active control of emulated tool vibration using a self-sensing actuator

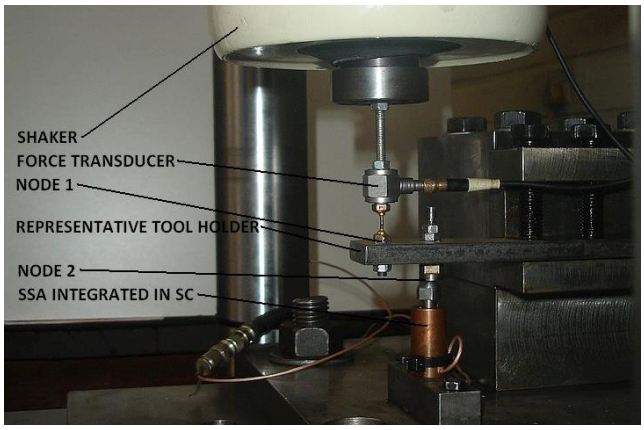

Fig2 Real image of test structure (Preference for color: online only)

Table 1 Equipment used in experimental set-up

Item	Type
Piezo drive amplifier	LE 500/200 voltage amplifier, Piezomechanik GmbH
Piezoelectric actuator	Stack actuator: PSt 500/10/15 VS18, Piezomechanik GmbH : $n = 50$, $K_a = 120\ N/\mu m$, $d_{33} = 450\ pm/V$
Electrodynamic shaker	Ling Dynamic Systems, V406/8
Shaker drive amplifier	Ling Dynamic Systems, PA100E
Force transducer	Model 208B02, PCB Piezotronics
Force transducer power unit	Model 480E09 ICP, PCB Piezotronics
Digital signal processor	TMS320C6713, Texas Instruments
Analog-to-digital converter	ADS 8361, Texas Instruments
Digital-to-analog converter	DAC 8554, Texas Instruments
Converter interface	5-6K Interface, Texas Instruments
Data acquisition card (DAQ)	PCI-6251 M-series, National Instruments
DAQ connector block	BNC-2110, National Instruments

The first bending mode of the strain gauge instrumented tool holder in tangential direction was at $1355.9\ Hz$.

Conversion of the measured signal into representative tool vibration signals for test purposes consisted of two steps and resulted in signals given in [dataset].

1. The instrumented tool holder's bending mode was shifted to the equivalent mode of the substitute tool holder with $2050\ Hz$ as the new centre frequency. The frequency ranges for each of the two signals were $100\ Hz$ and $200\ Hz$ of the measured signal with the first bending mode as centre frequency.
2. Low amplitude system noise replaced the frequency ranges outside these bands.

Control only targeted the tangential cutting force component. Authors of [6] did it in a similar way. This is briefly motivated as follows. In a turning process the magnitudes of the force component, tangential to the work piece, P_1 and two components, P_2 and P_3 orthogonal to it respectively in feed and radial direction stand in approximate ratios of $P_3 \approx 0.3P_1$ and $P_2 \approx 0.15P_1$ to $P_2 \approx 0.5P_1$ towards each other ([17]). P_1 increases the expected deflection for a standard tool holder due to a relatively high force-to-stiffness ratio in its direction. As a consequence this results in an increased tool work piece relative displacement with resulting surface roughness increase, hence the use of the force component tangential to the work piece as test signal. This is to stay with the main purpose of this study at this stage, which is focussed on a functionality test of the self-sensing actuator to control tool vibrations in an HIL-set-up.

2.1.3 Test procedure

The test procedure consisted of the following steps:

1. Balancing of the sensing circuit is done as described in subsection 2.2.2 about the sensing circuit balancing.
2. Shaker amplifier PA 100E volume dial needed to be set to 95% of its range to fully exploit the maximum force capability of the shaker.
3. The test signals, used for the HIL experiment, were the signals described in subsection 2.1.2. These constituted the data output from the National Instruments data card, installed in the desktop PC and listed in Table 1, to the driving amplifier of the shaker, PA 100E.

Two separate test runs, one for each bandwidth, with the sampling rate as that for model identification were performed.

4. The data card mentioned under point 3 was also used to capture data input. Acquisition of signal, V_{sens}, was performed when the controller embedded on the DSP was switched on and for comparison also once when the controller was switched off.
5. Above mentioned point 4 was performed for the test signal of 100 Hz bandwidth around the first bending mode of the representative tool holder and for the 200 Hz bandwidth signal around the same bending mode.

2.2 Sensing circuit and balancing

2.2.1 Circuit

Figure 3 shows the impedance bridge type sensing circuit (SC) block in Figure 1 in detail. From this single input single output (SISO) module, with several electrical time dependent variables as states, an output variable of interest in this work is V_{sens}.

V_{sens}, is proportional to the axial strain of the stack SSA. The strain of the SSA is the variable directly affected by the representative tangential cutting force induced disturbance on the tool holder substitute.

The SSA capacitance determines the parameterization of this circuit. Table 2 lists the parameters. The ratios $Z_{rp}/\ Z_1 = \ Z_p/Z_2$, with $Z_p = Z_{rp}$, are according to recommendations by [13]. The parallel resistors in the impedances Z_1 and Z_2 result in low-frequency roll-off for V_1 and V_2. Additional parallel capacitances in Z_{shunt} and $Z_{r\ shunt}$ increase the small inherent parallel capacitance of the high power shunts of Z_{shunt} and $Z_{r\ shunt}$ respectively to cause that the major voltage drop occurs across Z_p and its matching reference impedance, Z_{rp}.

This section furthermore provides a look into the theoretical basis of the sensing circuit output, i.e. the hardware building block output, V_o. Authors in [13] start with the formulation of this basis using the sensor equation, as

$$\theta_p\, r + C_p v = q_p \tag{1}$$

where $\theta_p = n\, d_{33}\, K_a$ with n, the number of layers in the stack, d_{33}, a piezoelectric constant and K_a the actuator stiffness. C_p is the actuator's capacitance, while r, q_p and v are the piezo actuator tip displacement, the charge on the piezo stack, and the voltage across its electrodes respectively.

If no charge from the stack actuator is lost, e.g. the piezo SSA is an open circuit, then the voltage, v, that appears across the piezo stack electrodes, becomes

$$v = -\theta_p\, r/C_p\ . \tag{2}$$

Compressing of the stack actuator by a displacement, r, generates the charge, q_p, on the electrodes of the piezo stack. Literature calls this the piezoelectric effect ([18]). In circuit diagrams, authors of [12] represent this effect as a voltage source.

The expression derivation for the output voltage of the impedance bridge, V_o, in [13] takes the piezoelectric effect into account. Here the second term of the expression for the voltage across the actuator and shunt, V_{act}, represents this effect:

$$V_{act} = V_{in} - V_2 = \frac{(Z_p + Z_{shunt})}{(Z_p + Z_{shunt} + Z_2)} V_{in} - \frac{Z_2 \theta_p\, r}{(Z_p + Z_{shunt} + Z_2) C_p} \tag{3}$$

Solving equation (3) from the derivation in [13] for V_2 and using voltage division in the reference branch to obtain V_1, results in $V_o = V_1 - V_2$. V_o is the output of the impedance bridge as

$$V_o = \left(g_1 Z_1 / \left(Z_1 + Z_{r\,p} + Z_{r\,shunt}\right) - g_2 Z_2 / \left(Z_2 + Z_p + Z_{shunt}\right)\right) V_{in}$$

$$-s g_2 \left(Z_2 Z_p / \left(Z_2 + Z_p + Z_{shunt}\right)\right) \theta_p r. \tag{4}$$

The gains for V_1 and V_2 are represented by g_1 and g_2 respectively. If the bridge is perfectly balanced and $g_1 = g_2$, V_o is represented by the second term of equation (4) only as

$$V_o = -Z_m(s)\theta_p r\ . \tag{5}$$

V_o, after becoming V_{sens}, becomes the feedback signal in the control system. The impedance bridge forms a current divider with two capacitive bridge legs and a purely resistive third leg. With these legs the current divider is fulfilling a low pass filter function. Authors in [19] put this insight forward to justify the extra purely resistive by-pass path in the bridge circuit. It serves to prevent a bias current in the capacitive legs. As a result of the current divider low pass filter, the current through the resistive leg becomes

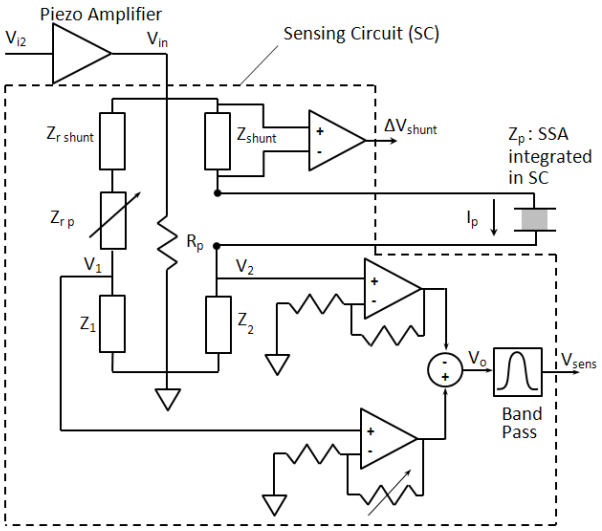

Fig3 Circuit diagram of sensing circuit with integrated SSA

Table 2 Impedance bridge and band pass data

Impedance bridge	
Impedance	Value
$Z_{r\,shunt}$, Z_{shunt}	$6\ \mu F\ ||\ 2.9\ Ohm$
$Z_{r\,p}$, Z_p	$207\ nF$
Z_1, Z_2	$2.2\ \mu F\ ||100\ Ohm$
R_p	$220 \cdot 10^3\ Ohm$
Band-pass	
Parameter	Value
Bandwidth	$\Delta\omega = 205 \cdot 2\pi\ rad/s$
Centre frequency	$f_o = 2050\ Hz$
Gain at f_o	$G = 1$
Quality factor	$Q = \Delta\omega/(2\pi f_o) = 10$

Table 3 Attenuation results of emulated tool vibrations

Bandwidth of representative force signal to shaker in [Hz]	Strain proportional amplitude of signal sensed by SSA at modal frequency	Amplitude in [N] of force applied to tip of representative tool holder at node 1	
	Maximum amplitude attenuation [%]	Without control	With control
100	70	1.03	1.03
200	65	0.97	0.97

$$I_R = \frac{(R_P C_B S+1)}{R_P C_B S}\, I_{in}\,, \tag{6}$$

where C_B is the total equivalent capacitance of the two capacitive bridge legs and I_{in} is the total current delivered to the impedance bridge.

2.2.2 Balancing

With a feedback control system unable to deal with noise in the feedback branch, this problem can mainly be addressed by maximizing the signal-to-noise ratio (SNR), ([20]). Therefore it is important to match the transducer and reference impedance as exact as possible. Impedance bridge matching was done using passive capacitors of XR7 material. In addition while the SSA is in a passive state, the signal of V_{sens} had to be minimized by adjusting the potentiometer to balance the bridge.

The next set of steps were to match the actuator, Z_p, and a passive capacitive impedance. In this way the differences in impedance due to the capacitors different dielectric materials was compensated for.

1. A passive capacitive impedance of XR7 material, Z_{rp}, matched Z_p. Equal capacitances and dissipation factors were the criteria and resulted in equal phase of V_2 and V_1.
2. A manually adjusted polystyrene capacitor compensated the mismatches between Z_{rp} and Z_p.

3. Theory/Calculation

3.1 Model identification and SSA linearization

The C-coded information that constituted the DSP application consisted of the AFANC algorithm and also the model coefficients. Mode finding and model identification of the control

system's forward path delivered these coefficients.

The following descriptive notation holds for the remainder of this work.

Abbreviation, $meas$:	refers to measured data.
Subscript, f:	refers to forward path frequency response function (FRF) or transfer function model.
Subscript, m:	refers to FRF used for mode finding.
Superscript, *:	refers to estimated FRFs, transfer models or finite impulse response (FIR) filters.
Symbols, F and T:	represent FRFs and transfer models respectively.

A sampling time of $4\ \mu s$, which corresponds to a $250 kHz$ sampling rate, the standard sampling rate for the external data converters, is the basis for the computation of the model coefficients for the AFANC filters. Less phase loss associated with the use of external data converters as compared to the on-board coder-decoder (codec) of the DSP was beneficial to an increased system phase margin.

3.1.1 Mode finding

A model of the path consisting of the digital signal processor (DSP), the voltage amplifier and the impedance bridge served as a linear parametric model for control purposes. However the force transducer and stinger caused a mass load effect on the representative tool holder and resulted in a shifted bending mode frequency of the tool holder. By adjustment the mass was determined and during model identification it was used to account for this effect.

The mode finding procedure consisted of the following iterative steps:

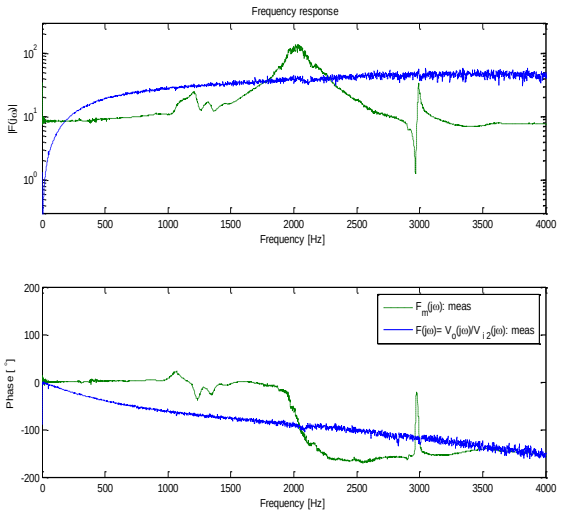

Fig4 FRF, $F_m(j\omega)$, for mode finding and FRF, $F(j\omega)$, of forward path section for mass load adjustment respectively

1. Application of a zero to $8000\ Hz$ bandwidth random noise to the shaker.
2. Measured signals by a dynamic force transducer and the SSA (not integrated in SC) to be used as I/O data for the FRF, $F_m(j\omega)$, in Figure 4.
3. FRF, $F_m(j\omega)$, in Figure 4 delivered the bending mode frequency of the substitute tool holder at $2050\ Hz$ while being connected to the shaker.
4. The shaker was then disconnected.
5. The first bending mode frequency could then be observed on an FRF $F(j\omega) = V_o(j\omega)/V_{i\,2}(j\omega)$ in Figure 4.
6. Adjusted the mass load at node 1, such that the frequency of the first bending mode seen in an FRF, $F(j\omega) = V_o(j\omega)/V_{i\,2}(j\omega)$ in Figure 4, would be as in step 3.

After applying the necessary mass load to shift the bending mode to $2050\ Hz$, one can see minor frequency effects at $2050\ Hz$ on $F(j\omega)$ in Figure 4. They are hardly visible due to other units such as the piezo amplifier and the impedance bridge on the same path of the FRF measurements.

3.1.2 Model parameter estimation

With knowledge of the bending mode from the third step in mode finding and mass load adjusted, as in the previous section, model identification could be performed. This could be done on the substitute tool holder disconnected from the shaker.

The decision was to use System Identification (SID) Toolbox from [21] instead of structure dynamical modelling software, since the general system under consideration is not purely structural but also electromechanical. Furthermore does the selected modelling software allow focus on stability, which is here a valid assumption due to the damping present in the structure.

The aforementioned path from the DSP with $V_{i\ dsp}$ as input, to the band-pass filter with V_{sens} as output, is here also called the forward path. It consists of several units in series and caused expectation for a higher order model for this path. A state space linear time invariant (LTI) type of model then provided the basis for the model structure. It is reliable, allowing for stable computer analysis algorithms ([22]).

The following aspects were the basis for conducting model parameter estimation:

Sampling rate:	It was selected as $100kHz$ and was above a minimum of at least 10 times the bandwidth of the control system in order to approach a continuous model ([23]).
Processing time:	It was accounted for by inclusion of the delay in the forward path data acquisition. The delay was caused by the processing on the DSP with time from input value assignment to output port variable assignment after the last algorithm instruction.
Input data, $V_{i\ dsp}$:	0 to 8000 Hz white noise input signal.
Output data, V_{sens}:	Anti-alias filtered acquisition of output data and its correction through inverse model of same filter.
Pre-processing:	Removal of the means from the output data and pre-filtering over the interval, $[1942 \quad 2149]\ Hz$.
Model selection:	The order selection option recommended a 6^{th} order state space model.
Estimation focus:	The focus was for stability and pre-filtered interval of the frequency range of interest.
Estimation method:	Prediction error method (PEM) ([24])
Model order reduction:	A lower order model being advantageous to the controller with removal of states hardly changing over time was adequate. The model was consequently reduced to a model of second order ([25], [22]).
Model:	

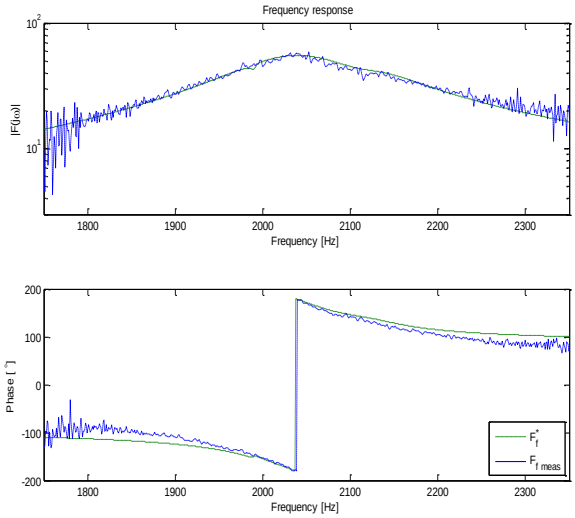

Fig5 FRFs for model of the forward path (dashed) and measurements of the same path (solid) respectively (Preference for color: online only)

$$T_f(z) = \frac{-0.03887\,z^2 - 0.1654\,z + 0.2036}{z^2 - 1.993\,z + 0.9956}. \quad (7)$$

Figure 5 shows the fit of the estimated model versus an FRF of the measured data for a narrow band only, since in this work, the control focus corresponds to this band.

The accuracy of this transfer function model is given by its percentage fit as

$$fit = 100\,(1 - \bar{\sigma}(\boldsymbol{y}_{m\,k} - \boldsymbol{y}_k)/\bar{\sigma}(\boldsymbol{y}_k - \bar{\boldsymbol{y}}_k)), \quad (8)$$

where $\boldsymbol{y}_{m\,k}$ is the simulated output of the model, $\boldsymbol{y}_k$ the measured output, $\bar{\boldsymbol{y}}_k$ its mean and the operator $\bar{\sigma}$ denotes the maximum singular value of the operand. The fit with the model in equation (7) yielded an accuracy of 85 % .

3.1.3. Linearization measures

3.1.3.1 Input voltage tracking by current in SSA

When a controlled output voltage amplifier drives piezoelectric actuators, the latter exhibit increased non-linear hysteresis ([19]). However non-linearity is negligible when a controlled current amplifier drives the actuators. The evaluation therefore was about the necessity to convert the available controlled voltage amplifier into a controlled current amplifier.

In addition to linearization, the controlled current amplifier offers the benefit of enhanced stiffness of the actuator. Documentation by [26] explains the reason behind this. Via the driving amplifier one therefore has control over the charge content on the piezo actuator, the electric field and consequently its stiffness ([27]). Two equations in the work of [13] illustrate this by means of the rewritten sensor equation (1)

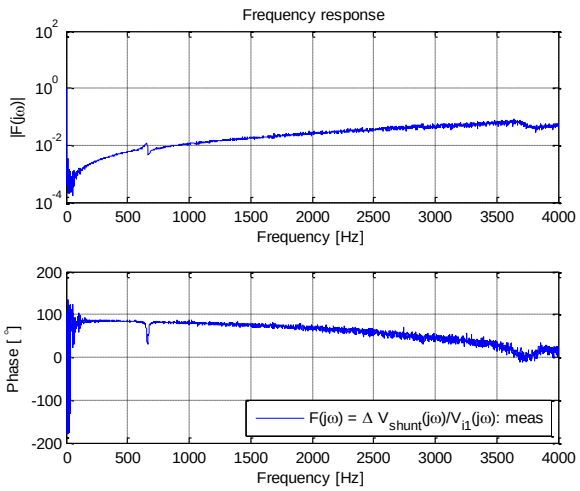

Fig6 FRF with V_{i1} as input and ΔV_{shunt} as output signal indicating phase of shunt current relative to V_{i1}

$$\theta_p\, r = q_p - C_p v\,. \tag{9}$$

Control and compensation of the charge to the SSA (i.e. the current) prevents charge leakage from the piezo stack, except for negligible internal leakage. This is the situation described by equation (2).

For this study a controlled current drive amplifier would mean that an inner feedback loop, as shown in the appendix in Figure 11, be implemented, such that the current in the piezo actuator would track V_{i1}. A $+90^{\circ}$ phase shift on ΔV_{shunt} , before feeding it back, can do this, assuming ΔV_{shunt} is in phase with the piezo amplifier input voltage, according to K.-H. Bayerle (personal communication, January 19, 2015).

For the set-up of this work the phase of ΔV_{shunt} at $2050\ Hz$ is already about 76° relative to the piezo amplifier input voltage, V_{i1}, as shown in Figure 6. It is therefore lagging V_{i1} by only 14° or less, when considering the actuator is not purely capacitive. For the purposes of this study this lag was sufficiently close to 0°.

3.1.3.2 Imposing of pseudo random noise

Imposing pseudo random noise on the control algorithm output, $\boldsymbol{u}_k$, formed a further measure to achieve linearization of the hysteresis found on piezoelectric actuators.

Each control algorithm output sample, u_k , added to a pseudo random noise sample as follows:

a. Generate a random number $n_{r\,k}$:

$$n_{r\,k} \in [-10, 10] \tag{10}$$

b. Obtain modified running mean m'_k :

$$m'_k = \left|\frac{K}{N}\sum_{j=k+1-L}^{k} u_j\right| \quad (11)$$

where $K = 5 \times 10^{-7}$ is a signal-to-noise-ratio (SNR) tuning factor and $N = 25$ is the window length for mean calculation.

c. Obtain random signal m_k proportional to m'_k:

$$m_k = n_{r\,k} \cdot m'_k \quad (12)$$

d. Filter $\boldsymbol{m}_k = [m_k, \ldots m_{k-L}]$ through two identical cascaded second order band pass filters, $G_{BP}(z)$, with centre frequency at $f_n = 110\,kHz$ and under-damped with damping ratio $\zeta = 0.1$. The purpose of these filters was to only allow narrowband noise through since only narrowband noise is necessary. The centre frequency is sufficiently high, but safely below the Nyquist frequency of the DSP sampling rate.

$$\boldsymbol{n}_k = G_{BP}(z) \cdot G_{BP}(z) \cdot \boldsymbol{m}_k, \quad (13)$$

where $G_{BP}(z)$ is the z-transform with the zero-order-hold and with

$$G_{BP}(s) = \frac{(2\pi f_n)^2}{s^2 + (4\zeta\pi f_n)s + (2\pi f_n)^2}\,. \quad (14)$$

e. The pseudo random noise, n_k then adds to the controller output value u_k:

$$v_k = u_k + n_k \quad (15)$$

where $V_{i1} = v_k$.

Imposing of pseudo random noise to the voltage applied to the piezoelectric actuator has an overall linearizing effect. Figure 7 shows this. By applying higher voltages, the extreme points of the loop become sharper and effects of hysteresis become visible ([19]). Pseudo

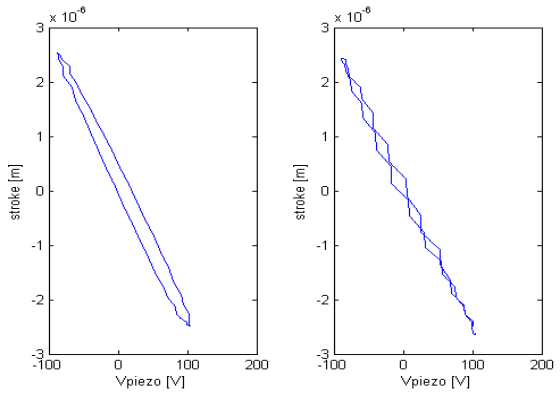

Fig7 Piezo stack actuator stroke vs. applied voltage without and with pseudo-random noise applied to V_{piezo} left and right graphs respectively

random noise then causes the more inflated hysteresis loop to partially collapse as shown in the right graph of Figure 7.

3.2 Control system

3.2.1 Method

As the commonly known regenerative effect occurs in turning process tool vibrations, it is valid to assume, that in turn this effect is also represented in the pre-recorded tool vibrations for this study. This is the connection to the machining process, besides the typical tool holder set-up, shown in Figure 1. As found in [28], these tool vibrations are non-stationary and require an adaptive algorithm, such as here the AFANC algorithm as control strategy. When used in a design of advanced stage, and being a feed-forward type of algorithm, its performance is superior compared to similar algorithms as shown in [29]. Due to limitations as addressed in section 4.3 the algorithm performance is limited in this study also.

In the remainder of this work it is the convention, that lowercase bold symbols represent vectors of delayed samples. The time instant of these vectors is indicated by the subscript, $\boldsymbol{k}$.

The control method as shown in Figure 1 encompasses a vibration control loop with feedback signal, V_{sens} . It is also represented as the block diagram shown in Figure 8. T_f is the transfer function of the forward path, i.e. the physical set-up given in equation (7), which includes the DSP, the voltage amplifier and the impedance bridge to the sensed bridge voltage, V_{sens}, as output. The signal sample $e_k = V_{sens\,k}$ is the sample sensed by the sensing circuit at time instance k and is the input to the control algorithm embedded on the DSP. The signal commanded by the control algorithm to the SSA, i.e. the output signal from the DSP at time instance, k, represents the sum of the signal samples u_k and n_k. Here n_k , discussed in the previous section, is the pseudo random noise imposed on the adaptive filter output, u_k.

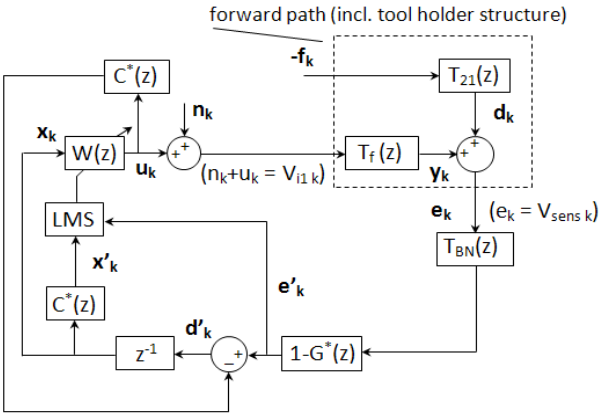

Fig8 Block diagram of control system based on AFANC

The forward path denotation is

$$T_f(z) = \frac{C(z)}{1-G(z)} \tag{16}$$

and $T_{21}(z)$ denotes the filter of the transfer function relating the input force, f_k, at node 1, at the tool tip, to the displacement resulting from that force, d_k, at node 2. Node 2 is the point of contact between the SSA and the bar representing the tool holder as indicated in Figure 1.

The input to the controller first undergoes a bias removal using the bias-notch filter

$$T_{BN}(z) = \frac{z-1}{z-0.995} \tag{17}$$

with a pole slightly left of the zero on the unit circle ([30]). Filter, $W(z)$, is a 16 tap adaptive finite impulse response (FIR)-filter.

Source [31] provided the C-code for the least-mean-square (LMS) section of the AFANC algorithm. An open-loop processor-in-the-loop (PIL) test on the DSP, also listed in Table 1, tested and verified the code. Two real-time data exchange (RTDX) channels for communication with a host PC's MATLAB workspace, using appropriate toolboxes [32], aided the testing. This was following an example in [31]. Simulation reached performance levels as in previously conducted work ([15]).

3.2.2 Algorithm

The DSP input and output signals in Figure 8 are $V_{sens} = e_k$ and $V_{i1} = u_k + n_k$ respectively. An adaptive FIR-filter, $W(z)$, determines the control action in the system as shown in Figure 8. The squared error expected value minimization, i.e. minimization of the cost function

$$J(w_i) = E\left[\boldsymbol{e}'_k \boldsymbol{e}'^{T}_k\right], \tag{18}$$

to search for appropriate w_i, the coefficients for the adaptive filter $W(z)$, and associated

minimization of $\boldsymbol{e}_k$ is used to derive the algorithm. This reduces the resultant displacement at node 2 (see Figure 1) caused by the cutting force acting at node 1 and the force exerted by the actuator on the tool holder structure. The choice of $\boldsymbol{d}'_{k-1}$ as the reference signal, instead of $\boldsymbol{e}_{k-1}$ as a reference, more effectively provides advance information about the primary noise, as it appears at the point of cancellation, which is node 2. This makes the adaptive feedback noise control (AFANC) algorithm, proposed by [16], preferred above the delayed error active noise control algorithm as used by [6]. Formulated in terms of a turning process, the primary noise is here represented as the tool holder deflection due to the cutting process. Here $\boldsymbol{e}_k$ was first pre-filtered by the denominator dynamics of the forward path, $1 - G^*(z)$, to cancel its poles and prevent them from participating in the coefficients', w_i, calculation. This is to avoid the instability when the poles migrate outside the unit-circle. This technique originates from literature ([33]). The pre-filtered error signal $\boldsymbol{e}_k$ is denoted as $\boldsymbol{e}'_k$, where

$$\boldsymbol{e}_k = \boldsymbol{d}_k + T_f(z)(\boldsymbol{u}_k + \boldsymbol{n}_k) \, . \tag{19}$$

Then, with $\boldsymbol{n}_k$ neglected, $\boldsymbol{e}'_k$, constructs as

$$\boldsymbol{e}'_k = \boldsymbol{d}'_k + (1 - G^*(z))T_f^*(z)W(z)\boldsymbol{x}_k = \boldsymbol{d}'_k + C^*(z)W(z)\boldsymbol{d}'_{k-1} \tag{20}$$

where $G^*(z)$, $T_f^*(z)$ and $C^*(z)$ are estimates of $G(z)$, $T_f(z)$ and $C(z)$ respectively.

In this work the objective was to directly keep the plant output zero. According to (20) the error $\boldsymbol{e}'_k$ then becomes

$$\boldsymbol{e}'_k = \boldsymbol{d}'_k \, . \tag{21}$$

A gradient descent algorithm is then used to update all the adaptive filter coefficients for the next time step, which is

$$\boldsymbol{w}_{k+1} = \boldsymbol{w}_k - \mu \frac{\partial J}{\partial \boldsymbol{w}_k} \tag{22}$$

where

$$\frac{\partial J}{\partial \boldsymbol{w}_k} = 2\boldsymbol{e}'_k \frac{\partial \boldsymbol{e}'_k}{\partial \boldsymbol{w}_k}\,. \tag{23}$$

The final updating equation for the coefficients w_i , with $i = 1,2 \ldots L$ and L the length of filter $W(z)$, becomes

$$\boldsymbol{w}_{k+1} = \gamma\, \boldsymbol{w}_k \, - \alpha\, \boldsymbol{e}'_k C^*(z) \boldsymbol{d}'_{k-1}. \tag{24}$$

Equation (24) is also known as the filtered-x LMS algorithm because the FIR filter $C^*(z)$ filters the feedback type reference signal, $\boldsymbol{x}_k = \boldsymbol{d}'_{k-1}$ and becomes the gradient of the algorithm. The leakage coefficient γ is here assigned the value 0.99. The work of [6] states that it improves the systems robustness. The coefficient $\alpha = 2\mu$ is a convergence coefficient ([34]). It is determined as

$$\alpha = \frac{\tilde{\alpha}}{L\overline{\boldsymbol{x}'^{\,2}_k}} \tag{25}$$

where $\overline{\boldsymbol{x}'^{\,2}_k}$ is the mean-square of the filtered reference signal, $\boldsymbol{x}_k$. According to [34] $\tilde{\alpha}$ should be

$$0 < \tilde{\alpha} \, < 2\,. \tag{26}$$

The choice in this work is that $\tilde{\alpha} = 0.02$, since lower values for a convergence coefficient are recommended for models that do not have an exact fit.

4. Results and Discussion

4.1. Attenuation

The magnitude attenuation of V_{sens} in dB, in the upper two graphs of Figure 9, is also quantified in Table 3. This reduction achievement is at the first bending mode at $2050\ Hz$. With control on a sideband on the high frequency side occurred however hardly exceeding the magnitude of the attenuated vibration. The sideband occurrence is due to inferior model fit outside the targeted narrow bands of $100\ Hz$ and $200\ Hz$.

In comparison with desktop PC simulation under ideal conditions, the result was a 93 % attenuation. It was achieved without unidirectional form locking limitation, i.e. with form locking for pushing and pulling and with an exact model for the controller. This shows the need for bidirectional positive form locking at the actuator-tool-holder connection and for model accuracy.

Results in Figure 9 and Table 3 show that with the force for the controlled and the uncontrolled case unchanged, the SSA has reacted with stiffness variations to the variations of the input disturbance force. The latter was downscaled to approximately 25% of the tangential force's dynamic component for a hard turning example of a real process ([35])

With an input sinusoidal amplitude of $2V$ peak-to-peak applied to the shaker amplifier PA 100E (volume dial set to 95% of its range), Figure 9 (lower graph) shows that the sensed signal, V_{sens}, reaches a signal-to-noise-ratio (SNR) of 20 dB (i.e. $20 \log\ (50/5)$).

In comparison [36] suggests that for the feedback path in process control, consisting of communication channels between a plant and master station, the minimum required SNR be $4\ dB$.

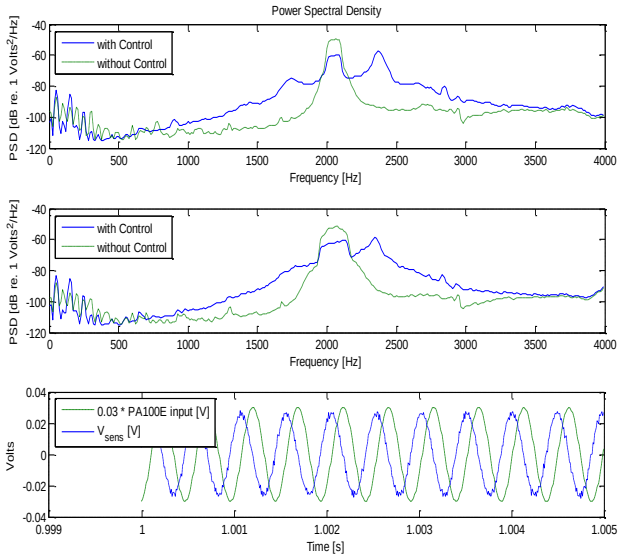

Fig9 PSD of V_{sens} for a 100 Hz and a 200 Hz bandwidth test signal (upper and middle graphs respectively) and SC sensed signal, V_{sens}, with PA 100E input signal (lower graph)

4.2. Post-experiment measurements

With the post-experiment measurements it was the intention to also investigate the controller output. This however happened after damping increased and input-output coherence decreased due to a reassembled set-up. A possible reason for the latter could be slight loss of contact of the SSA tip at node 2 as indicated by the change in input-output coherence.

With re-estimation of model parameters the gain and real value slow zero of the forward path model was modified to have values of similar order of magnitude as the model in (7). This enhanced responsiveness of the controller utilizing this model.

In Figure 10b) two neighbouring signal frequency components explain the beating phenomenon in the controlled output in Figure 10a). The control effort in Figure 10c) is toward setting the controller output frequency to the one sensed, i.e. V_{sens}. Here it is clear that the controller output is in this case restricted by the output voltage limits of the digital-to-analogue converter. This may partly be attributed to the indirect position of the SSA with respect to the node of application of the disturbance, which is the representative cutting force. Partly it can also be attributed to the aforementioned unidirectional form locking limitation.

The levels to which active control has attenuated emulated tool vibrations in the upper graph of Figure 9 and Figure 10b), i.e. $60\ dB$, are comparable. However in case of Figure 9, the attenuation was due to active control only, while in Figure 10b) it was due to a combination of structurally induced passive damping as well as active control.

4.3. Limitations to performance

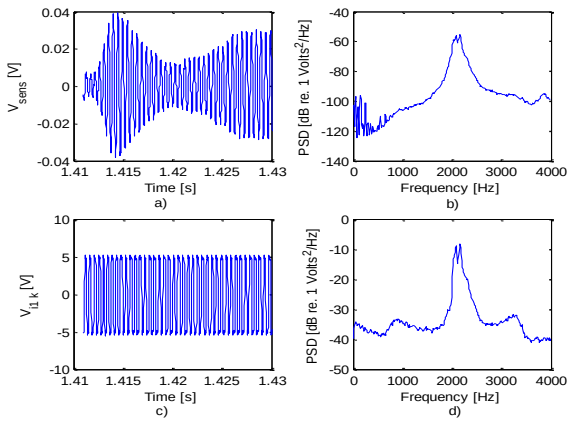

Fig10 Time domain and PSD of SSA sensed signal, V_{sens} respectively in a) and b) and equally for the controller output, V_{i1}, respectively in c) and d)

Elimination of the following limitations can further improve the control system performance, as presented in this functionality test.

1. As only the SSA's pushing action ensured contact of the SSA and substitute tool holder, it limited positive form locking to that particular direction. However in this study the use of an electro dynamic shaker in the set-up required a zero static force. This consequently required a form locking for both pushing and pulling action of the SSA. This is unlike a real turning process, where the static force is non-zero and, due to forced contact, a form locking for the pushing action only would suffice. However as a conservative precaution a specially designed mechanical connection would prevent loss of contact of the actuator for the pulling action. In this study the connection point of the actuator and the tool holder has no form locking in pulling direction with the purpose to allow cant of the tool holder relative to the actuator. This protected the piezoelectric stack from cant itself and consequently damage.

2. In order to first reach and demonstrate first stage system functionality, model identification was limited to a narrow band in this HIL set-up and resulted in adequate performance limitation to the frequencies within the respective band only.

3. Associated with the dual function of the SSA are two requirements that have to be met. Firstly the SSA's position in the structure should enable a high signal-to-noise-ratio (SNR) regarding its sensor function, i.e. avoid noise in the feedback path due to a closed-loop system inability to control it there ([20]). Secondly and simultaneously as an actuator the control is most effective if its actuation on the controlled variable is as directly as possible ([37]). This study, for its purposes, only considers the first requirement through bridge balancing, reference matching and through SSA position selection. The aim here was increased measurability of the deflection at node 2 by the SSA. Associated with the concept of this study, this particular challenge was not found as addressed in literature so far.

4. The total noise at a point of the tool holder on the opposite side of node 2, which will here be called node 3, consists of noise by the cutting force exerted at node 1 plus superimposed noise that originates from the non-linearity of the actuator such as loss of contact and remaining actuator hysteresis. This would be hysteresis, which has not completely been linearized. Noise from the loss-of-contact type non-linearity is a clear mechanical design issue and can be rectified by appropriate design. A clear picture of the remaining noise situation, not investigated here, may however be obtained by exerting a sinusoidal force signal at node 1, which is the point of action of the cutting force. The resulting deflection is then measured using a laser vibrometer at node 3 with the passive SSA still part of the set-up. However the SSA should then be mechanically

connected at node 2 in a way that guarantees bidirectional form locking. A similar measurement by a vibrometer at node 3 is recorded when a sinusoidal force signal of equal frequency and amplitude measured at node 3 is exerted by the SSA at node 2. The latter can then be either modelled or compared visually to the former measurement to establish its proportion of the total noise.

4.4 Competitive technologies

4.4.1 Established technologies

Table 4 gives an overview of the technology of tool active vibration control (AVC) using a self-sensing actuator as proposed in this study and two competitive technologies respectively in the 2nd, 3rd and 4th columns. These technologies are here compared according to criteria referring to the control strategy of each and also their practicality. Table 4 shows that the control concept discussed in this paper compares favourably with competing technologies based on the criteria used here.

4.4.2 Artificial neural network technologies

In the now accelerating research in deep learning, there are two approaches using artificial neural network active vibration control methodologies that should be mentioned. The first one is from 2010 and uses, similar to the approaches mentioned in section 4.4.1 also a piezo actuator to counteract tool vibrations. The second approach is not yet an active tool vibration control application from 2017 but is applied to general active vibration insulation.

In the first approach, mentioned in [43], a multilayer feedforward ANN model is trained via resilient backpropagation to represent the plant. For the collection of network training data

Table 4 Comparing competitive piezoelectric actuator based tool AVC technologies

Tool AVC type:	This study's AVC: Self-sensing with impedance bridge sensing circuit/ AFANC algorithm [16]	AVC of [38]: Self-sensing/ adaptive Positive Position Feedback (PPF) control	AVC of [6] Seperate sensor and piezoelectric actuator/ FxLMS algorithm [6]
Criteria:			
Feedback	Position/deflection (absolute position control)	Position/deflection (absolute position control)	Acceleration (jerk control)
Stability	Root locus remaining in left-half s-plane [39]	Root locus remaining in left-half s-plane [39]	Not guaranteed because non-collocated
Design & add-ons	Sensing circuit safe from harsh conditions	Sensing segment and actuator on same stack	Accelerometer
Practicality	External turning plus boring	External turning	External turning plus boring
Control direction	Tangential	Radial	Tangential
Control strategy	Adaptive LMS-type	Adaptive using self-tuning regulator (STR)	Adaptive LMS-type
Forward path type	General model	Second order model	General model
Performance/ convergence	Trade-off between robustness and convergence via algorithm step-size [40]	Slow convergence [41]	Trade-off between robustness and convergence via algorithm step-size [40]
Robustness	See convergence trade-off	Robust [42] [38]	See convergence trade-off
Algorithm implementation	Simple	Requires additional STR	Simple
Frequency range	Broadband [16]	Mainly modal frequencies	Narrowband
Efficiency	10 dB plus room for improvement pointed out	10 to 16 dB	40 dB

the plant is the tool holder structure with the actuator position as point of input and the accelerometer position as output, while the primary disturbance is kept equal to zero. During training network weights are adjusted so as to minimize the difference between the ANN model output and the real plant output. For AVC the model is used in its inverse form. A control signal is sent to the actuator via the inverse ANN model. It is produced by using the plant output as input to the inverse ANN model to counteract the plant's primary source of vibration.

The delay caused by processing is estimated and reversed in the control signal such that current rather than previous plant output disturbances are targeted. However with this application the sinusoids in the plant output disturbance are targeted in sequential iterations rather than simultaneously as in the HIL tests of the current studies. The approach of [43] achieves a performance of 73 % attenuation of the maximum disturbance amplitude. The advantage of this approach is that it is robust and the model can accommodate non-linearities of the plant.

The second ANN approach in [44] is a general vibration insulation application, which can however be applied to turning tool dynamics by omitting the intermediate base plate in the dynamic model. This is a later application of ANN in AVC which makes use of sliding mode control combined with a radial basis function (RBF) network. This type of network was chosen because of its quick learning ability. Sliding mode control was brought in as a non-linear continuous control. It is clear how the switching surface derivative was chosen to approximate the switching surface maintaining a non-zero lower bound. This was done to reach the sliding mode, and thus reduced dynamics, in finite time. It also meets a Lyapunov requirement for stability.

A performance of 77 % attenuation of the maximum white noise disturbance amplitude was achieved with required robustness properties.

5. Conclusion

This concept's application and content of this work is the control of emulated tangential tool vibrations with an SSA and active control algorithm. The control system's implementation as HIL incorporates a hardware building block with an integrated SSA. It also included a software building block accommodating the AFANC control algorithm and data of the identified path with the tool holder model.

The suggested method has shown that the complete HIL system was functional with sufficiently high signal-to-noise-ratio for the control system feedback signal. It shows a performance, of up to 70% attenuation when targeting the substitute tool holder bending mode vibrations of 100Hz bandwidth. The actuator current lagging the voltage input to the driving amplifier by only a small phase angle, is a proof of sufficient linearity support. It was also confirmed that pseudo random noise enhances linearity for larger strokes of the SSA. Post-experiment results confirmed that the control action indeed targets the frequency of the first bending mode of the substitute tool holder.

The purpose of this study was to develop a complete control system for emulated tangential tool vibration, and prove its functionality. It now serves as a basis to reach the stage of market readiness. This work has established that the control system is feasible for further development.

Aforementioned requirements for its sensor- and actuator function recommend a specific SSA position choice in the structure for a real turning process implementation.

References

[dataset] Freyer, BH, Theron, NJ, Heyns, PS, & Pickelmann, LA (2016) Self-sensing active tool vibration control input signals. Mendeley Data, v2. http://dx.doi.org/10.17632/smxz6dcr3d.2

[1] Pratt, JR, & Nayfeh, AH (1999) Design and modeling for chatter control. Nonlinear Dynamics, 19(1), 49-69.https://doi.org/10.1023/A:1008322520352

[2] Chiou, RYS, & Liang, SY (1999) Chatter frequency in turning considering tool compliance and wear land. J Manuf Sci Eng, Trans ASME, 121(2), 927-941. https://doi.org/10.1115/1.2831221

[3] Bonifacio, MER & Diniz, AE (1994) Correlating tool wear, tool life, surface roughness and tool vibration in finish turning with coated carbide tools. Wear, 173(1-2), 137-144. https://doi.org/10.1016/0043-1648(94)90266-6

[4] Byrne, G, Dornfeld, D, Inasaki, I, Ketteler, G, König, W, & Teti, R, (1995) Tool condition monitoring (TCM) – the status of research and industrial application. Ann CIRP, 44, 541-567. http://dx.doi.org/10.1016%2FS0007-8506(07)60503-4

[5] Cho, D-W, Lee, SJ, & Chu, CN (1999) The state of machining process monitoring research in Korea. Int J Mach Tools Manuf, 39, 1697-1715. https://doi.org/10.1016/S0890-6955(99)00026-7

[6] Andrén, L, Håkansson, L, & Claesson, I (2003) Active control of machine tool vibrations in external turning operations. Proc Inst Mech Eng [B], 217(6), 869- 872. https://doi.org/10.1243/09544050360673251

[7] Pan, J, & Su, C-Y (2001) Modeling and chatter suppression with ultra-precision in dynamic turning metal cutting process. Proc DETC'01 ASME Des Eng Tech Conf, Pittsburgh, PA, 9-12 September, 6 B, 1125-1132.

[8] Rakotondrabe, M (2013) Combining self-sensing with an unkown-input-observer to estimate the displacement, the force and the state in piezoelectric cantilevered actuators. Am Control Conf (ACC), Washington, DC, USA.

[9] Cole, DG, & Clark, RL (1994) Adaptive compensation of piezoelectric sensoriactuators. J Intell Mater Syst Struct, 11, 263-271. https://doi.org/10.1121/1.408890

[10] Carabelli, S & Tonoli, A (2000) System properties of flexible structures with self-sensing piezoelectric transducers. J Sound Vib, 235(1), 1-23. https://doi.org/10.1006/jsvi.1999.2913

[11] Peterman, JS, & Clark, RL (1995) Hybrid analog and digital adaptive compensation of piezoelectric sensoriactuators. Proc AIAA/ASME Adapt Struct Forum, New Orleans, LA, 2854-2859. https://doi.org/10.2514/6.1995-1098

[12] Dosch, JJ, & Inman, DJ (1992) A self-sensing piezoelectric actuator for collocated control. J Intell Mater Syst Struct, 3, 166-185. https://doi.org/10.1177/1045389x9200300109

[13] Anderson, EH, & Hagood, NW (1994) Simultaneous piezoelectric sensing/actuation: analysis and application to controlled structures. J Sound Vib, 174(5), 617-639. https://doi.org/10.1006/jsvi.1994.1298

[14] Freyer, BH, Heyns, PS, & Theron, NJ (2014) Comparing orthogonal force and unidirectional strain component processing for tool condition monitoring. J Intell Manuf, 25, 473-487. https://doi.org/10.1007/s10845-012-0698-6

[15] Freyer, BH, Theron, NJ, & Heyns, PS (2008) Simulation of tool vibration control in turning, using a self-sensing actuator. J Vibration Control, 14(7), 999-1019. https://doi.org/10.1177/1077546307085389

[16] Kuo, SM, Kong, X, & Gan, WS (2003) Applications of adaptive feedback active noise control system. IEEE Trans Control Syst Technol, 11(2), 216 – 220. https://doi.org/10.1109/tcst.2003.809252

[17] Koenigsberger, F (1964) Design principles of metal - cutting machine tools. NY: Pergamon Press Limited, p.5.

[18] Roddeck, W (2003) Einführung in die Mechatronik. Stuttgart: B.G. Teubner GmbH, p.11.

[19] Moheimani, SOR, & Fleming, AJ (2006) Piezoelectric transducers for vibration control and damping. London: Springer-Verlag Limited.

[20] Dorf, RC, & Bishop, RH (2005) Modern control systems (10th ed.). Upper Saddle River, N J: Pearson Education, Inc., p.204.

[21] MATLAB (2007) System Identification Toolbox Version 7.1. [computer software]. Natick MA: The Mathworks Inc.

[22] MATLAB (2003) User's Guide of Control System Toolbox Version R13 [software documentation]. Natick MA: The Mathworks Inc.

[23] Lutz, H, & Wendt, W (2002) Taschenbuch der Regelungstechnik. Frankfurt am Main: Verlag Harri Deutsch, p.667.

[24] Ljung, L (1987) System identification – Theory for the user. Englewood Cliffs, NJ: Prentice Hall Inc., p.171.

[25] Föllinger, O (1990) Regelungstechnik. Heidelberg: Hüthig Buch Verlag GmbH, p.585.

[26] Pickelmann, L (2010) Piezomechanics: An Introduction. Company broschure, Piezomechanik GmbH. Retrieved from http://www.piezomechanik.com/en/introduction Accessed 12 August 2016

[27] Heimann, B, Gerth, W, & Popp, K (2001) Mechatronik. Munich: Fachbuchverlag Leipzig im Carl Hanser Verlag, p.56.

[28] Sturesson, P-OH, Hakansson, L, & Claesson, I (1997) Identification of statistical properties of cutting tool vibrations in a continuous turning operation - correlation to structural properties. Mech Syst Sig Process, 11(3), 459-489. https://doi.org/10.1006/mssp.1996.9998

[29] Haase, F, Lockwood, S, & Ford, DG (2003) Active vibration control of machine tool structures - Part 2: An experimental active vibration control system, Trans Eng Sci Vol.44. https://doi:10.2495/LAMDAMAP030391

[30] Widrow, B, & Stearns, SD (1985) Adaptive signal processing. NY: Prentice Hall, p.323.

[31] Chassaing, R (2005) Digital Signal Processing and Applications with the C6713 and C6416 DSK. Hoboken, N J: John Wiley & Sons, Inc.

[32] MATLAB (2006) Computer Software Version R2006b [Toolboxes: Simulink, Signal Processing Toolbox, Link for Code Composer Studio, Signal Processing Block Set, Embedded Target for TI C6000 DSP(tm)]. Natick MA: The Mathworks Inc.

[33] Vipperman, JS, Burdisso, RA, & Fuller, CR (1993) Active control of broadband structural vibration using the LMS algorithm. J Sound Vib, 166(2), 283-299. https://doi.org/10.1006/jsvi.1993.1297

[34] Elliott, SJ (2001) Signal processing for active control. London: Academic Press Limited.

[35] Scheffer, C, Kratz, H, Heyns, PS, & Klocke, F (2003) Development of a tool wear-monitoring system for hard turning. Int J Mach Tools Manuf, 43, 973-985. https://doi.org/10.1016/s0890-6955(03)00110-x

[36] Jović, F (1986) Process control systems: principles of design and operation. London: Kogan Page Ltd., p.367.

[37] Ogata, K (1970) Modern Control Engineering. Englewood Cliffs, N J: Prentice Hall, Inc., p.7.

[38] Radecki, PP, Farinholt, KM, Park, G, & Bement, MT (2010) Vibration Suppression in Cutting Tools using a Collocated Piezoelectric Sensor/Actuator with an Adaptive Control Algorithm, J Vib Acoust 132(5):051002. https://doi.org/10.1115/1.4001498

[39] Preumont, A (2002) Vibration control of active structures: An introduction. Dordrecht: Kluwer Academic Publishers, second edition, p.78.

[40] Ravinchandra, KA/L, Fei, TK, & Yong, LC (2019) Active Noise Reduction using LMS and FxLMS Algorithms, J Phys : Conf Ser 1228:012064. https://doi:10.1088/1742-6596/1228/1/012064

[41] Orszulik, R, & Shan, J (2011) Multi-Mode Adaptive Positive Position Feedback: An Experimental Study, Am Control Conf (ACC), O'Farrell Street, San Francisco, CA, USA, June 29 - July 01

[42] Moheimani, SOR, Vautier, BJG, & Bhilkkaji, B (2005) Multivariable PPF Control of an Active Structure, Proc 44th IEEE Conf Decis Control, and Eur Control Conf Seville, Spain, December 12-15

[43] Xia, Y (2010) Experimental implementation of artificial neural network-based active vibration control and chatter suppression. Ryerson University, Canada, Theses and dissertations, Paper 869.

[44] Yang, L, Su, K, Liu, S, Wu, H. & Li, H (2017) 2729. Study on active vibration isolation system using neural network sliding mode control. Int. Ltd J Vibroengineering, 19(8), ISSN 1392-8716. https://doi.org/10.21595/jve.2017.15195

Appendix A

This section describes the inner control loop option as a control loop with feedback signal, V_I. The purpose of the feedback via a phase shift in Figure 11 is to carry out enhanced tracking of the input voltage V_{i1} by the current in the piezo actuator shown as I_p in Figure 3. The inner control loop is an additional option and measure to linearize the hysteresis exhibited by the piezoelectric actuator.

K.-H. Bayerle (personal communication, January 19, 2015) suggested this configuration. Instead of directly sensing the current in the piezoelectric actuator, I_p, the voltage difference over the shunt in Figure 3, ΔV_{shunt}, indicates its magnitude. A-priori knowledge that the phase of current in the piezo element is $90°$ relative to the phase of ΔV_{shunt}, indicates the phase of I_p .The phase shift block in Figure 11 indicates that if the phase of ΔV_{shunt} relative to V_{i1} is φ° , then a $-(\varphi - 90)°$ shift of phase would be needed on ΔV_{shunt} . Phase equality of the feedback signal and the current in the piezo actuator is the reason for this requirement. In Figure 11 the signal V_I in Volt is equal to I_p in Ampere.

If the magnitude of the open loop path G_{ip} is set to

$$\left|G_{ip}\right| = \frac{|I_p|}{|V_{i1}|} \approx 1 \tag{A1}$$

by selection of R_{shunt} with

$$\left|I_p\right| = \frac{|\Delta V_{shunt}|}{R_{shunt}} \ , \tag{A2}$$

and the inner loop feedback system notation in Figure 11 is T_{ip}, then it derives as

$$T_{ip} = \frac{2G_{ip}}{1+G_{ip}} \tag{A3}$$

with V_{i1} as input and V_I as output.

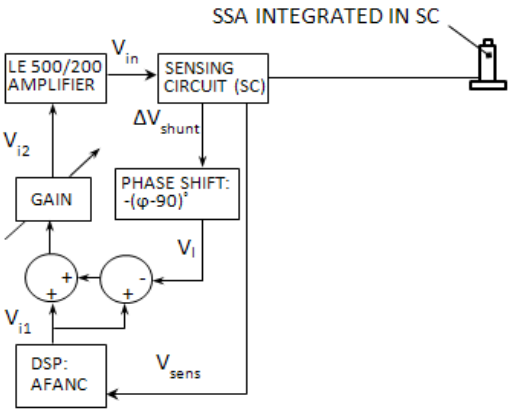

Fig11 Control system with inner SSA current control loop